Control of GMAW: Detection of Discontinuities in the Weld Pool

Ultrasonic pulses transmitted into the base of the weld pool detect discontinuities and signal parameter changes

BY N. M. CARLSON, J. A. JOHNSON AND D. C. KUNERTH

ABSTRACT. Ultrasonic methods were used to detect incomplete sidewall fusion, porosity and weld bead geometry in molten steel pools formed during gas metal arc welding of T-joints and single-bevel V grooves. A dual-element, piezoelectric transducer mounted on the base metal transmitted ultrasonic pulses into the region at the base of the weld pool. The returning echoes were shown to be indicative of the geometry of the pool and of the presence of incomplete fusion and porosity. Two analysis methods, based on ray tracing and transducer field calculations, were used to confirm the experimental results. An expert system was proposed to analyze the returning echoes and to provide information about the weld pool to an intelligent controller that determines when the welding process parameters need to be changed. A noncontacting ultrasonic system was discussed as a potential practical alternative to the contact system used in this work.

Background

In a research program at the Idaho National Engineering Laboratory (INEL), methods of sensing the physical properties of the weld during gas metal arc welding (GMAW) are being evaluated as part of the development of an automated GMAW system. In this system, properties of the weld would be controlled using the feedback from the sensors as input to a model of the welding process that relates these properties to welding parameters. This paper describes the portion of that work relating to the use of ultrasound to detect weld defects as they are being made. Ultrasonic techniques are shown to be capable of obtaining information from the region in and around the molten weld pool that relates to the formation of incomplete sidewall fusion and porosity.

N. M. CARLSON, J. A. JOHNSON and D. C. KUNERTH are with Idaho National Engineering Laboratory, EG&G Idaho, Inc., Idaho Falls, Idaho

This information can be sent to the controller, which then makes decisions about how the welding process should be altered to prevent further discontinuities from forming.

A diagram of an automated welding control scheme is shown in Fig. 1. On the left are the various types of sensors capable of detecting the physical properties of the weld. These sensors may be categorized by type — infrared, electrical, optical and ultrasonic — or according to the properties of the welding process they measure, such as pool geometry (optical and ultrasonic), cooling rate (infrared), droplet formation mode (electrical), and discontinuities (ultrasonic).

Infrared sensors can be used to detect cooling rate, which is important for control of fracture toughness while maintaining strength in some steels (Ref. 1). Workers at Auburn University are also using infrared techniques for pool size and tracking measurements (Refs. 2,3).

Electrical signals include variation in current and voltage, as well as the standard DC values. Variations provide information on transfer mode of droplets detaching from the melting wire (Refs. 4, 5). This is important, since for many applications the spray transfer mode (Ref. 6) is required for quality welds and the boundary between this transfer mode and other, undesirable modes may shift due to factors beyond the control of the system.

KEY WORDS

GMAW Control
Discontinuity Detection
Weld Pool Discontinuity
Fillet Welds
Single Bevel Vs
Incomplete Penetration
Sidewall Penetration
Ultrasonic Methods
Weld Test Methods
NDE Expert Systems

Optical techniques such as the INEL vision system can be used for joint tracking and fitup measurements, as well as for observing the shape and size of the top surface of the molten pool and the droplet detachment (Ref. 7). Richardson at Ohio State University has developed a vision system that views the pool through a special hollow torch body, providing some of the same information as the INEL vision system (Ref. 8). Ultrasonic methods are also being used to determine the pool geometry at the molten/solid interface. (Ref. 9). Initial experiments were performed by Lott (Ref. 10) at INEL and Katz and Hardt at MIT (Ref. 11). Fenn and coworkers at Brunel University claim to have used ultrasonic measurements to determine the depth of joint penetration and to control that depth by varying the welding current in submerged arc welding (Ref. 12). Unfortunately, insufficient detail was presented in their papers to confirm or repeat their results.

The final sensor in Fig. 1, which is the topic of this paper, uses ultrasound to detect discontinuities in the weld pool during welding. The ultrasonic echoes from the molten/solid interface and the molten pool provide information about the quality of the fusion zone and the molten pool. Unacceptable welding conditions that can result in porosity, incomplete sidewall fusion or undercut are detected.

Other sensors are also being used, which are not listed on the control-scheme diagram. These include spectroscopic and photometric measurements of the arc for penetration control (Ref. 13), real-time radiography for discontinuity detection (Ref. 14), and measurements of the audible sound emitted by the process for droplet transfer mode detection (Ref. 5)

The column labeled Analysis in Fig. 1 is where the raw sensor data are converted into the desired information on the process, such as cooling rate deduced from the raw infrared data. This information is passed on to two intelligent modules, which use the information to determine the best method of filling the weld while

maintaining the correct heat input to the weld. These modules contain economic constraints as well as physical ones since the fill strategy determines the number of passes required to fill the joint and thus the productivity of the process.

The final step is a model of the welding process, which converts the requested heat and fill inputs to the physical welding parameters (Ref. 15). Both Hardt (Ref. 16) and Eagar (Ref. 17) at MIT are also working on aspects of modeling GMAW, including the control scheme required for a nonlinear, cross-coupled system and the physical aspects of the wire melting.

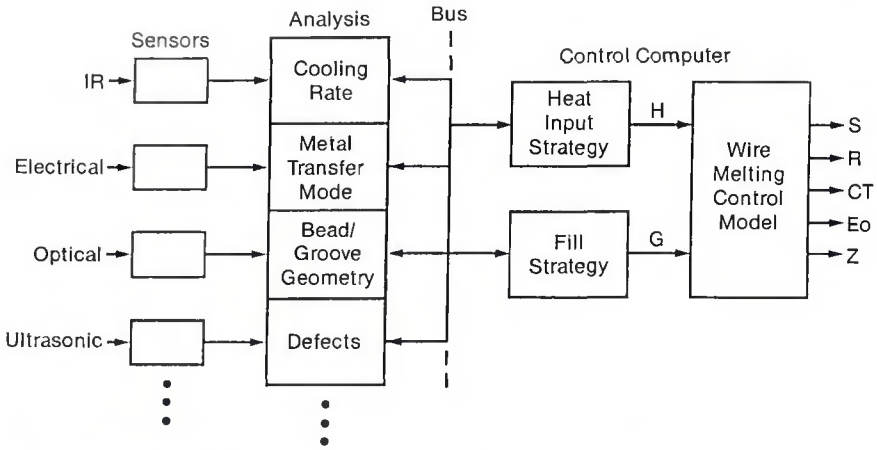

Fig. 1 — Conceptual diagram of the parts of an automated GMAW system.

Preliminary Experiments

An initial study was conducted to determine the capability of longitudinal acoustic waves to detect discontinuity conditions in the molten weld pool during GMAW. Refracted longitudinal waves were used primarily because they can propagate into the molten weld pool and thus allow inspection of the pool's interior during the welding process.

A single-element, 5-MHz piezoelectric transducer, operated in the pulse-echo mode, was mounted on a Lucite wedge such that 45-deg refracted longitudinal waves were generated in a 25.4-mm (1.0-in.) thick carbon steel sample. The transducer was positioned 25.4 mm from the top edge of a 90-deg sidewall preparation so that the 45-deg longitudinal wave was directed into the bottom corner of the weld preparation and was moved in alignment with the electrode throughout the welding pass — Fig. 2. The other side of the preparation was at a 60-deg bevel. The two parts were tacked together with a 6.35-mm (0.25-in.) steel backer bar with a 4.5- to 8.0-mm (0.18- to 0.31-in.) root opening at the bottom of the preparation. A-scan signals from two flaw generating conditions (porosity and incomplete sidewall fusion) and from a good weld (Fig. 3) were acquired.

Incomplete sidewall fusion was achieved by mistracking the welding gun relative to the joint and simultaneously increasing the contact-tube-to-workpiece distance from 15.9 mm (0.63 in.) to approximately 25 mm (1.0 in.) and decreasing the wire-feed rate. To achieve porosity, a fitting with a septum was added to the argon shield gas line that permitted the injection of a volume of air into the cover gas. The final quality of the weld was determined by radiographic techniques for these preliminary tests.

The first A scan in Fig. 3 shows echo signals from the benign, geometric reflectors in the weld preparation prior to welding. These reflectors include the bottom corner (Reflection B), the sidewall preparation (Reflection C), and internal reflections from the Lucite wedge (Reflection A).

The second A scan in Fig. 3 shows that when the root pass penetration is adequate and the molten pool is aligned with the transducer, no significant reflectors are observed from the bottom corner or the sidewall preparation. Since incomplete sidewall fusion had occurred on the root pass (third A scan), the bottom corner signal was still present because the corner geometry was not significantly altered by the welding process. Porosity (fourth A scan) in the molten weld pool resulted in a set of dynamically changing reflections that occurred later in time than the original bottom corner reflection. The last three A scans in Fig. 3 can be discriminated visually, which implies that an expert system could be developed to distinguish these three welding conditions (Ref. 8, 18).

This initial study demonstrates that refracted longitudinal waves can provide information about two unacceptable welding conditions, porosity and incomplete sidewall fusion. However, multiple reflections introduced by the transducer wedge provide no information about the welding process and complicate signal interpretation. To understand the source of the received signals, analysis techniques are needed to model the interaction of the sound waves with the molten pool and the weld preparation. Also, both radiography and destructive evaluation are required to determine accurately the quality of the weld at locations of interest. Thus, a series of additional experiments are planned that will address these shortcomings.

Experimental Procedures

Improvements were made in the ultrasonic transducer and in the evaluation of the results for these experiments. The major difficulty in the preliminary experiments was the presence of the echoes from the internal reflections in the Lucite wedge. To overcome this difficulty, a dual-element transducer was designed and purchased. In this transducer, two 12.7-mm (0.5 × 0.5-in.) square piezoelectric elements were mounted on separate Lucite wedges that were next to each other but electrically and acoustically isolated. One element served as a transmitter and the other as a receiver. The reflections from inside the transmitting wedge were not observed in the receiving wedge. The two elements were angled slightly toward each other so that the centers of the sound beams intersect at a point 25.4 mm (1.0 in.) deep in the carbon steel base metal. This point is at the bottom corner of the 90 deg weld preparation because the angle of refraction was again chosen to be 45 deg — Fig. 4. Both elements were matched to have a broadband frequency response centered at 5 MHz.

The transducer was kept in a fixed position and data were acquired during welding at 0.32 mm intervals as the electrode moved along the weld preparation

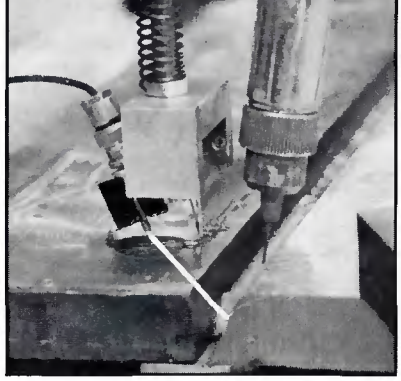

Fig. 2 — Single element 45 deg refracted longitudinal transducer aligned with electrode on single bevel V-groove weld sample.

past the transducer. An encoder was mounted on the side-beam welding machine to measure the position of the electrode. Thus, the position of the electrode relative to the transducer was known and the formation and solidification of the weld pool, as well as the pool itself, could be observed. The electrode position was recorded, the transducer was pulsed and the echo data were digitized using a computer-controlled workstation (Refs. 19, 20).

Two different weld preparations were used. The first, a single-bevel V groove, was the same as was used in the preliminary experiments described above. The second was a fillet weld of 25.4-mm steel on a 6.35-mm steel bar. However, ultrasonically the geometries of the two preparations were identical as the transducer is mounted on the 90 deg corner portion of both samples. In fact, the bevel side of the groove specimens often was not fused to the backing bar and did not appear in some of the sample photos of the destructive evaluation.

GMAW was performed using a Linde side-beam welding machine and a Cobramatic wire feeder. The welding parameters were: currents from 212 to 310 A, voltages from 22 to 28 V, travel speeds from 0.23 to 0.27 m/min (9.1-10.6 in./min), and wire feed rates of 7.9 to 12.4 m/min (311 to 488 in./min) using 1.1-mm (0.045-in.) diameter welding wire. The average deposition rate was 1.4 g/s (11 lb/hr). The spray transfer mode was used with a contact-tube-to-workpiece distance of 15.9 mm (5/8 in.) The shielding gas was 98% argon and 2% oxygen.

The flaw types generated for these experiments were incomplete sidewall fusion and porosity. The incomplete sidewall fusion was generated as before by mistracking, increasing the contact-tube-to-workpiece distance, and reducing the wire feed speed. Porosity was generated by manually fanning the cover gas. The porosity obtained with this technique was very gross compared to that obtained in the preliminary experiments. Undercut on the sidewall adjacent to the top of the fill was made by mistracking the electrode up the sidewall.

Destructive evaluations of the welds were made at 26 transducer locations on weld root passes to determine the quality of the weld for correlation to the acquired ultrasonic data. The welds were cut perpendicular to the preparation in a plane containing the transducer sound centerline. The destructive evaluations showed the geometry of the weld pool and the presence of both near-and-far-side incomplete fusion, acceptable sidewall fusion, and porosity.

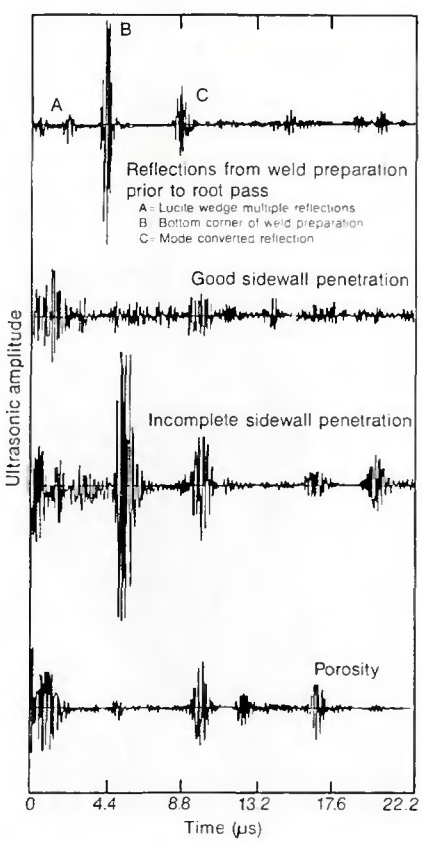

Fig. 3 — A scans of weld preparation prior to and during the root pass of good and flawed welds acquired with a single element transducer.

Ray-Tracing and Sound Field Calculations

Echoes were received from the sidewall preparation prior to the root pass and from the weld pool as the electrode passed the transducer. During welding, the echoes from the preparation may be reduced in amplitude or changed in shape because the molten metal penetrates the sidewall and changes the reflectivity of the sidewall. To understand the sound paths of the signals received before and during welding, two methods of analyzing the data were used to validate the arrival times and relative amplitudes of received signals and to determine the sound path in the experimental data.

In the first method, rays were traced from the point where the ultrasound entered the part, to various reflectors on the preparation and in the weld pool, and then to where the ultrasound exited the part at the receiving transducer. A computer program was written to trace these rays, accounting for the refraction of the ray as it entered or exited the molten pool and for the change in the angle of reflection upon mode conversion (change in sound mode from longitudinal to transverse and vice versa). The input to the computer program consisted of the number of rays, information on whether the ray is reflected or transmitted when it reaches a boundary, the mode of the ray on each leg, and the sound speeds of the longitudinal and transverse wave modes in the two media (solid steel and molten steel). No attempt was made to account for the effect of the temperature gradients near the solid/molten interface. Although these gradients are known to affect the sound speed and distort the sound field slightly (Ref.21), such calculations are complex and are not needed for identification of the wave paths observed in the data. The output of the program consisted of the locations of each entry and reflection point of the ray, the transit time for each leg, and the total transit time for the ray.

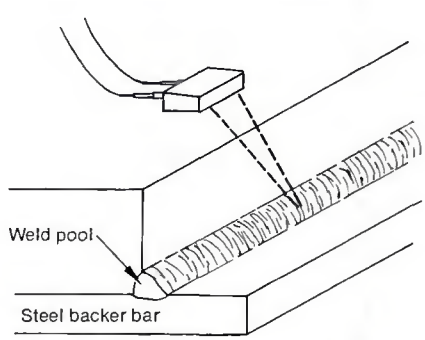

Fig. 4 — Schematic of the center rays from the dual-element transducer.

Two versions of the program were used. In the first, the user entered the initial angle of the ray at the entry point and observed the path of the ray on a graphics terminal. In the second version, the program iterated through initial angles until the final leg exited at the location of the receiving transducer.

In the second analysis method, another computer program (Ref. 22) was used to determine the approximate beam spread of the sound field. The program calculated the field due to a transducer coupled to the solid through the plastic wedge with a thin layer of fluid couplant. In this technique, the transducer face was divided up into many small areas, each of which was assumed to be a source of spherical waves. A ray was traced from each source point, through the wedge and into the solid to the requested field point. The vector sum of the fields of each of the rays was then calculated to find the total incident field at that point for a particular frequency.

From the field of the transducer, the relative amplitudes of the signals were determined. Using this code the magnitude of the sound field at locations along the bottom surface of the weld sample (x direction) and along the sidewall preparation (z direction) was calculated for the transducer placed on the steel sample at coordinates ($x = -25.4$, $z = 25.4$). The calculated longitudinal beam spread was defined to be the area between the points where the amplitude of the field was down by 20 dB relative to its maximum value along the beam centerline. Note

that the centerline for transverse waves from this transducer was at an angle of 27 deg in the steel part, while the angle for longitudinal waves was 45 deg. For the longitudinal waves these 20-dB points are at (x = −11, z = 0) in the x direction (on the bottom of sample, 11 mm from the bottom corner), and at (x = 0, z = 10) in the z direction (up the sidewall, 10 mm from the corner). Between these positions along the bottom and up the sidewall the ultrasonic field was down by less than 20 dB compared to the field at the centerline of the transducer. For the refracted transverse beam, the beam spread along the bottom (x direction) was 10 to 23 mm (0.4 to 0.9 in.) from the bottom corner with no significant sound field on the vertical sidewall. Because of reciprocity, the effect of the beam spread on the amplitude of a received signal from a given point was expected to be the same as that on a transmitted signal to the same point.

Experimental Results before Welding

An A scan of the unwelded part is shown in Fig. 5. Three large signals can be seen and their source can be identified using the two analysis techniques described above. The results of ray-trace analysis of this unwelded preparation are shown in Fig. 6. The sound entrance and exit points were 25.4 mm from the edge of the 25.4-mm-thick carbon steel weld sample. Only the base metal on the 90 deg side is shown since the backing bar and the base metal on the 60 deg side were not acoustically coupled to the first piece. In Fig. 6A, a direct longitudinal wave at 45 deg reflecting from the corner is shown. This ray is actually made up of three legs: one from the transducer to the corner, one across the corner and one returning to the transducer. The second leg is too short to be seen in the figure. For simplicity, the ray is called the L-L ray, meaning that it consists of two longitudinal legs. The coordinates in the x-z plane of the entry and exit points and the reflection point are shown in the figure. The ray moves to some extent in the direction perpendicular to the plane of figure corresponding to the distance between the center of the sending and receiving elements — Fig. 4. The ray-trace program calculated the total time for this ray to be 15.6 μs (including the transit times in the two wedges of the dual-element transducer). This correlates well with the first echo observed in the A scan in Fig. 5. The L-L signal to the corner is obviously along the centerline of the transducer and should be a large reflection in the acquired A scan.

Fig. 6B shows a more complicated path consisting of an initial transverse ray at 27 deg, which mode converts at the bottom surface to a longitudinal ray. This intersects the sidewall preparation at 8.4 mm and reflects to the top surface entering the Lucite wedge at a final angle of 56 deg. This path is called T-L-L (meaning transverse-longitudinal-longitudinal). The reverse of this path is also possible. The predicted time for this ray is 19.8 μs. This path correlates well with the second echo in Fig. 5. The T-L-L path should have a large amplitude since both the initial and final rays are within the beam spread of the transducer. The initial transverse leg (or final transverse leg for the reverse path) intersects the bottom at −12.5 mm (−0.5 in.) well within the beam spread of the transducer. The final (or initial) longitudinal leg intersects the sidewall at 8.4 mm (0.33 in.) up from the bottom corner and the 20-dB point is at 10 mm (0.04 in.) up from the bottom corner.

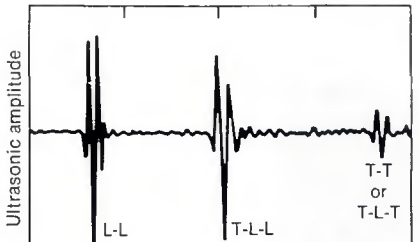

Fig. 5 — A scans of weld preparation acquired with dual element transducer.

Fig. 6C shows another path, L-L-T, generated by an initial longitudinal leg at 34 deg that reflects off the bottom and mode converts to a transverse wave at 12.5 mm up the sidewall. This wave enters the Lucite wedge at an angle of 63 deg. The total time for this ray is also 19.8 μs, the same as the T-L-L ray. However, the L-L-T path is not expected to have a large amplitude. The initial longitudinal ray arrives at the bottom at 8.4 mm from the corner, within the 20-dB limit of the beam, but the final transverse ray originates from a position on the sidewall well beyond the transverse wave beam spread of the transducer. A similar analysis shows that the reverse of this ray is also expected to be small.

Other rays that are expected to be small in amplitude include a T-T ray, which is similar to the L-L ray shown in Fig. 6A, and a T-L-T ray, which consists of an initial transverse ray to the bottom surface at 14.8 mm that mode converts to longitudinal, intersects the weld preparation at 14.8 mm, and mode converts back to transverse (T-L-T). Both these rays have total travel times of 25 μs. The reflection received from the T-T ray is not expected to be of significant amplitude since the corner at 25.4 mm is outside the beam spread for both the initial and final transverse legs. Finally, in the case of the T-L-T combination, the transverse ray to or from the sidewall is beyond the beam

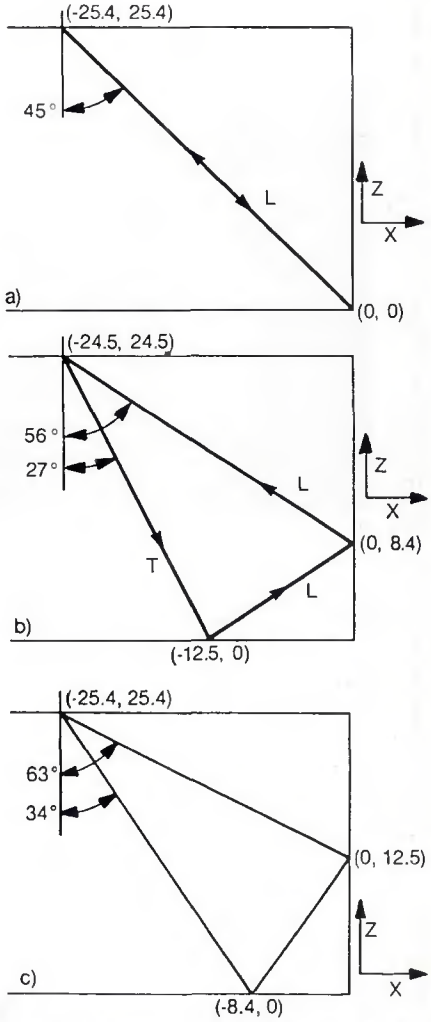

Fig. 6 — Traces for rays before welding. A — L-L ray path; B — T-L-L ray path; C — L-L-T ray path

spread of the transducer for transverse waves and the signal is not expected to be large. In Fig. 5, this ray is observed, but it is smaller than the other two discussed above and is not observed in all preweld sidewall preparation A scans. The reasons for this are not clear and may be related to the roughness of the preparation.

Experimental Results during Welding

Digitized data and destructive evaluations were obtained for a total of 26 locations on root weld passes. Photomicrographs and A scans for five of these weld locations are presented in Figs. 7–11. The weld shown in Fig. 7 is a fillet weld. The others are single bevel V-groove welds — the bevel side did not fuse to the backing bar and came off during destructive evaluation in the examples shown in Figs. 9 and 11. These examples illustrate the signals obtained for a good weld (Fig. 7), unacceptable welds (Figs. 8–10) and one very poor weld — Fig. 11. These signals were analyzed to determine if incomplete

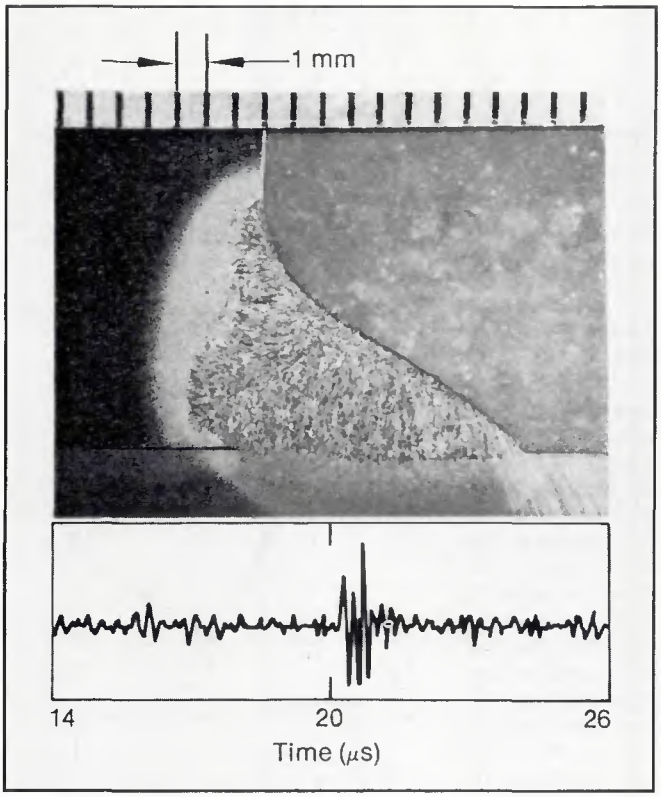

Fig. 7 — Polished and etched weld sample of adequate sidewall penetration and fill height with A scan acquired during the root pass.

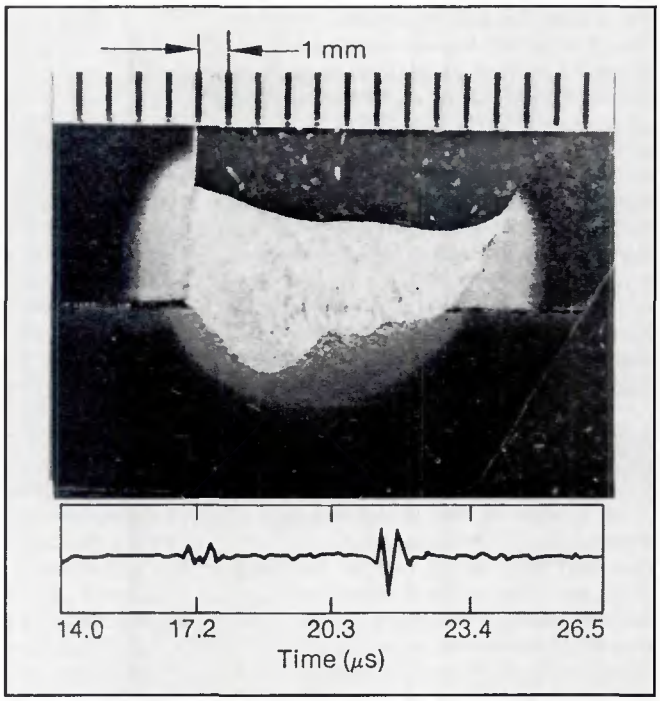

Fig. 8 — Polished and etched weld sample of adequate sidewall penetration and low fill height with A scan acquired during the root pass.

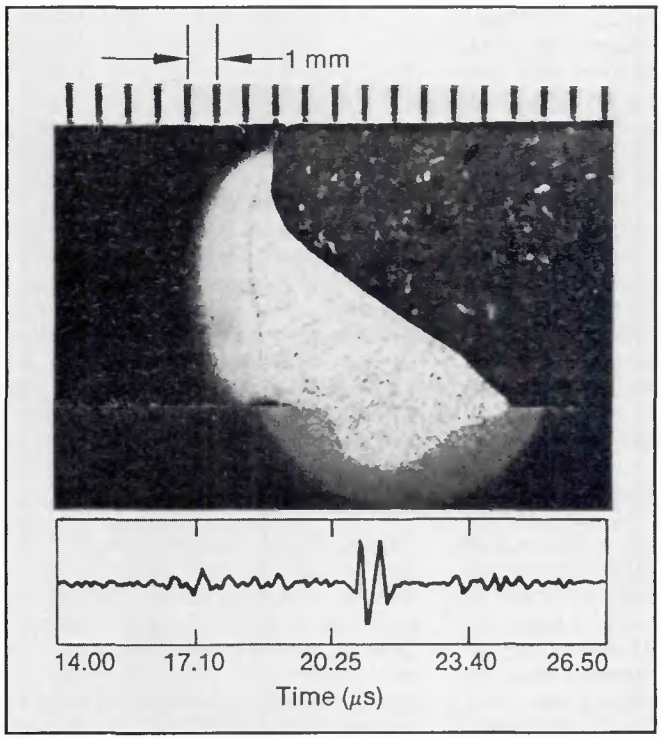

Fig. 9 — Polished and etched weld sample of incomplete penetration with A scan acquired during the root pass.

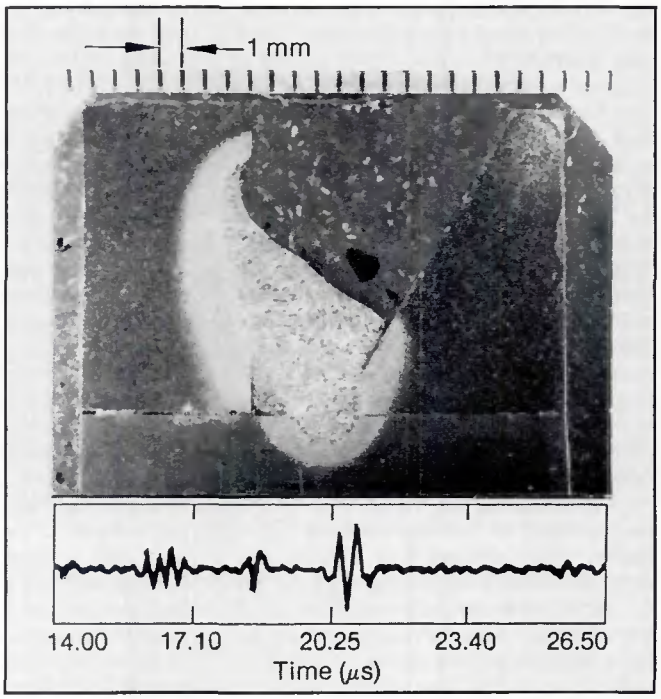

Fig. 10 — Polished and etched weld sample of near and far side incomplete penetration with A scan acquired during the root pass.

penetration, porosity or undercut conditions could be detected by observing the changes in the signals due to the various sound paths in the weld sample. The A scan below each photomicrograph is of the digitized acoustic signal as the molten weld pool passed the transducer. The results obtained from the ray trace and field code analyses were used to understand the echoes in the digitized signals.

The molten pool affected the three signals from the weld preparation (Fig. 5) in various ways. Consider first the L-L signal. When adequate sidewall penetration occurred, the longitudinal wave refracted at the molten interface with the majority of the sound entering the pool and with little sound energy returned to the receiving element. The amplitude of the signal reflected from the molten/solid interface can be calculated from the impedances of the two media. The impedance in turn depends on the sound speed and density of the material. For solid and molten steel at the melting point the sound speeds, densities and impedances are (Ref. 23):

	Solid	Molten
Velocity	4.8×10^3 m/s	4.05×10^3 m/s
Density	7.8×10^3 kg/m^3	6.88×10^3 kg/m^3
Acoustic impedance	37.4×10^6 Ns/m^3	27.9×10^6 Ns/m^3

The amplitude reflection coefficient, R, can be calculated from the impedances, Z, by:

$$R = (Z_s - Z_m)/(Z_s + Z_m) = 0.146$$

Thus, with adequate penetration, the L-L echo should be only 14.6% of its preweld amplitude in Fig. 5. Higher amplitudes occur only if the penetration is not complete. If discontinuity conditions like inadequate sidewall fusion were present, the effective impedance over the area of the incomplete fusion is zero, resulting in all sound energy being reflected from the discontinuity at an angle favorable for reception by the receiving element. Actually, because of the increase in attenuation of sound with temperature, the reflected amplitude from a sidewall with good penetration is expected to be significantly less than that predicted from the reflection coefficient.

Now consider the effect on the T-L-L ray. The centerline of this ray intersects the sidewall 8.4 mm from the bottom corner. Thus, this ray path can be affected by sidewall fusion or undercutting higher than 8.4 mm.

Complete sidewall fusion with adequate fill is achieved in the weld shown in the photomicrograph in Fig. 7. In the A scan acquired from the molten pool, the signal from the L-L ray to the bottom corner is not observed as the longitudinal waves enter the pool because adequate sidewall fusion is achieved and no sound is reflected back to the transducer. The fill height of 8.5 mm is sufficient to alter the waveform of the T-L-L ray at 20 μs since this ray intersects the sidewall at 8.4 mm.

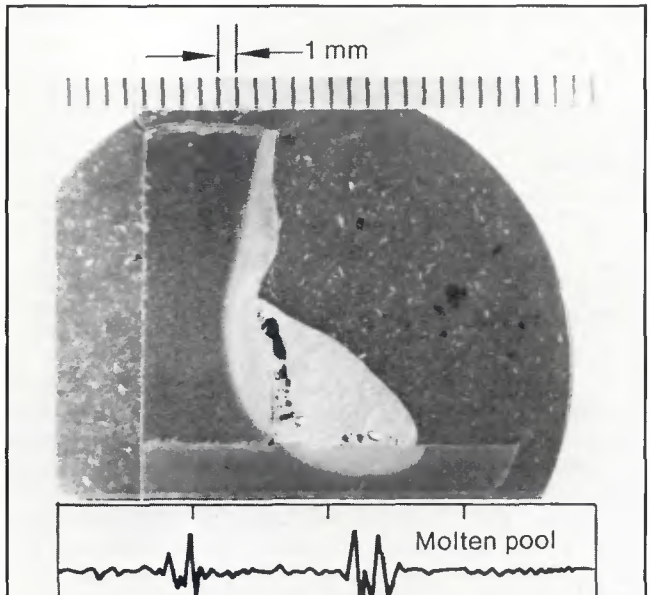

Fig. 11—Polished and etched weld sample of porosity, undercut and incomplete penetration with A scan acquired during the root pass.

Complete penetration of the bottom corner is shown in Fig. 8, but with a low level of only 4 mm. The L-L signal is small but present and the waveform is different than that observed before welding—Fig. 5. This is due to the fact that the corner reflector is still present because the low fill level of this root weld does not affect all of the rays that contribute to the L-L sound path. Figure 12 shows that at this low fill level about 60% of the L-L beam is sending and receiving sound energy from the corner. In addition, the T-L-L ray is not affected by this weld because the fill level is well below the centerline of the returning L wave.

Incomplete penetration of the bottom corner is shown in two examples. The first (Fig. 9) example is of incomplete fusion of the backup bar but full fusion of the sidewall. The L-L signal has a very low amplitude, indicating acceptable sidewall fusion, and the waveform of the T-L-L is not altered since the fill level is below the centerline of the beam. The bottom corner reflection appears to indicate a complete fusion condition, which is not the case in this weld as the backup bar is not penetrated. Therefore, this technique is not appropriate for determining the quality of penetration for the backing bar but only the quality of fusion at the sidewall.

Figure 10 shows a root pass with both incomplete sidewall fusion and undercut. Incomplete fusion is evident in the A scan since the L-L signal from the corner, although decreased in amplitude, is still a significant reflector. In this case the fill height of 11 mm (0.43) is sufficient to affect the corner reflector rays that have a ray path to 10 mm in the z direction. Therefore, the bottom corner reflection can only be due to the presence of corner geometry caused by incomplete sidewall fusion at the root of the weld. The T-L-L wave is affected in a minor way by the 11 mm fill height and the undercutting at 12 mm, indicating that this fill geometry is not one that alters this path very much.

A new signal, between the L-L and T-L-L, appears in the A scan in Fig. 10. Using the ray tracing program, this is determined to be due to the path shown in Fig. 13. The angle of the molten pool is such that the surface of the pool is a specular reflector that returns the ray shown in Fig. 13 directly back to the transducer at the time observed in the A scan.

In Fig. 11, incomplete fusion, porosity and severe undercutting caused by an

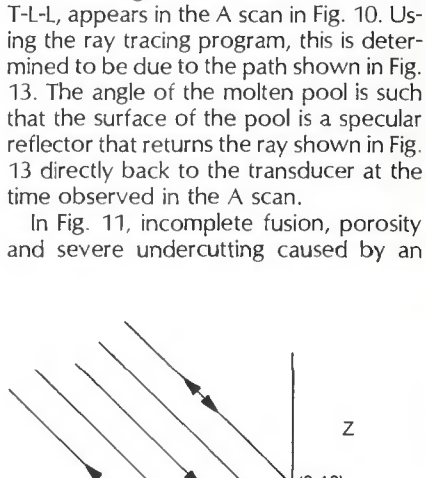

Fig. 12—L-L ray paths in the presense of a molten pool showing some rays transmitted into the pool and others returning to the transducer.

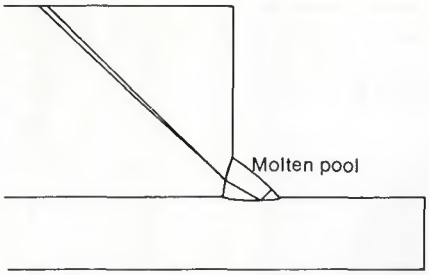

Fig. 13 — Ray path that accounts for the presence of the extra echo observed in the weld shown in Fig. 10.

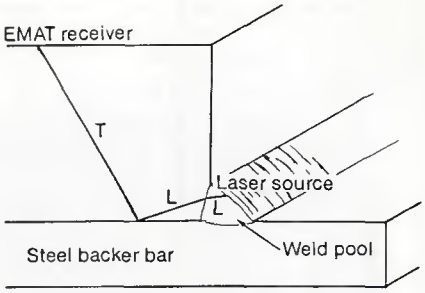

Fig. 14 — Schematic of noncontacting sensing of fill level of a fillet weld.

unacceptable welding process are shown. The bottom corner reflector (L-L) remains when the molten pool is present, indicating the incomplete sidewall fusion, although the fill height is adequate. This means the corner reflection is due to incomplete fusion and not low fill level as in Fig. 8. The T-L-L signal is reduced in amplitude and the waveform altered dramatically because of severe undercutting and gross porosity at the sidewall.

Discussion

Ultrasonic Discontinuity Detection

The analysis of data acquired during root passes from 26 stationary transducer locations shows that certain discontinuity conditions can be detected using refracted longitudinal sound waves to interrogate the molten pool. Severe undercut above 8 mm can be detected by the T-L-L path, because of the distorting effect the undercut has on the signal. Furthermore, this distortion can be observed as a decrease in the amplitude of the signal and a change in the waveform. Incomplete fusion can be detected if it occurs at the sidewall. However, incomplete fusion of the backing bar is not detected using the current experimental setup.

Expert System Potential

An expert system could be used to determine discontinuity conditions during GMAW. By first recording the initial weld preparation signals using a dual-element ultrasonic transducer and then monitoring the signals observed during welding for the presence of an L-L signal with a large amplitude and waveform changes in the T-L-L signal, the system could make decisions about the presence of discontinuity conditions and the quality of the weld geometry. The expert system would then provide an input signal to a closed-loop process control system to minimize the amount of unacceptable root weld from the automated welding process. The system could work like one already developed for use in ultrasonic evaluation of solidified, partially completed welds (Ref. 24). In that system, a simple "If, Then, Else" type of logic is used to evaluate the amplitude and shape of ultrasonic signals and decide if the A scan contains echoes from incomplete sidewall fusion, porosity or good weld. The system is an expert system in the sense that the decision process is based on the same cues in the A scans that the developers of the system were able to use to discriminate among the different flaws and good weld.

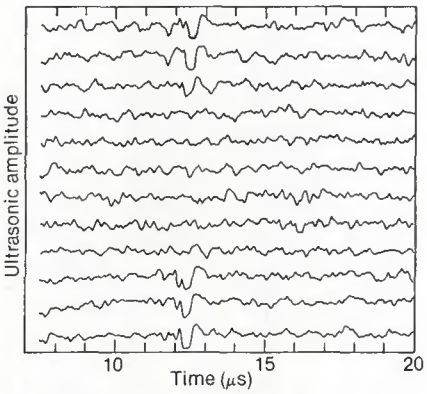

Fig. 15 — Noncontacting ultrasonic data showing the effect of low fill level.

Noncontacting Ultrasonic System

To make the system truly practical, difficulties in using the piezoelectric transducers must be overcome. The major problem is the maintenance of coupling between the transducer and the part. This is normally done with a film of gel between the Lucite wedge and the part. This gel must be fairly thin and uniform with no gaps or large bubbles. In the preliminary experiments, a special fixture was built to provide a continuous flow of gel between the transducer and the part for the short (1-m) distances of travel. Stroud (Ref. 25) uses more complex devices which maintain coupling by pumping gel into a tube, which then takes the place of the plastic wedge.

Another approach is to use noncontacting transducers (Ref. 26). In preliminary experiments on fillet welds, a laser spot was focused on the molten weld via mirrors and lens to generate ultrasound directly on the surface of the weld pool (note the laser energy was much less than that used in laser beam welding). The ultrasound was transmitted through the pool to an electromagnetic acoustic transducer (EMAT) on the part as shown schematically in Fig. 14. With this experimental setup, the sound path went through the molten/solid interface about 3.9 mm (0.15) up the sidewall and was therefore affected by low fill level. When the fillet weld geometry was acceptable, sound generated by the laser was received by the EMAT. Figure 15 shows a sequence of A scans obtained at 8-mm intervals with this noncontacting system, starting in an area of adequate fill level, passing through an area of low fill level, and then back to adequate fill level. The signal received by the EMAT at 12 μs through the sound path shown in Fig. 14 was initially present, disappeared in the region of low fill level, and then returned as the acceptable fill level was restored. Starting with the fourth A scan, a severe drop in fill level resulted in the disappearance of this signal. This occurred because the change in the fillet weld geometry alters the sound path to the EMAT to such an extent that no sound was received. As an acceptable fill level was again achieved, the EMAT received a signal from the weld as seen in the last three A scans of Fig. 15.

For this noncontacting system to be fieldable, several improvements must be made. The EMAT is much less sensitive than piezoelectric transducers and the signals in Fig. 15 show a poorer signal-to-noise ratio than those presented above for the piezoelectric transducer (Fig. 5, Figs. 7–11). An order of magnitude improvement in sensitivity is required for practical use. The laser beam must be delivered to the weld via a fiber-optic cable to reduce personnel hazards in the work area and to increase the mobility of the source of excitation on the weld for interrogation of the total weld interface. Using only mirrors and lenses, sound could be generated only on the upper part of the weld pool.

Conclusions

Discontinuities may be detected during GMAW using ultrasonic methods. The types of discontinuities detected in this work are incomplete sidewall fusion, gross porosity and undercut. The information about the position and types of discontinuities being formed could be derived from the ultrasonic signals by an expert system and the results sent to the controller of an automated GMAW system. The controller could change the welding parameters to prevent the continuation of the discontinuity condition, thus improving the quality of the welding process. In addition, the conditions leading to defects may also be detected (Ref. 9), and the potential exists for preventing the discontinuity conditions altogether. Noncontact-

ing systems may improve enough in the future to provide a very practical means of implementing the technique on the shop floor.

Acknowledgments

This work was supported by the U. S. Department of Energy, Office of Energy Research, Office of Basic Energy Sciences under DOE Contract No. DE-AC07-76IDO1570. Appreciation is expressed to U. S. Wallace who overcame his pride to make welds with flaws deliberately and to G. L. Fletcher who prepared the destructive evaluation samples.

References

1. Lukens, W. E., and Morris, R. A. 1982. Infrared temperature sensing of cooling rates for arc welding control. *Welding Jour.* 61(1):27-33.

2. Govardhan, S. M., and Chin, B. A. 1989. Monitoring GTA weld puddle geometry using measured surface temperature gradients. Recent trends in welding science and technology TWR'89. *Proceedings of the Second International Conference on Trends in Welding Research,* Gatlinburg, Tenn. pp. 383-386.

3. Nagarajan, S., Groom, K. N., and Chin, B. A. 1989. Infrared sensors for seam tracking in GTAW. Recent Trends in Welding Science and Technology TWR'89, *Proceedings of the Second International Conference on Trends in Welding Research,* Gatlinburg, Tenn., pp. 951-955.

4. Lui, S., and Siewert, T. A. 1989. Metal transfer in gas metal arc welding: droplet rate. *Welding Journal* 68(2):52-s to 58-s.

5. Johnson, J. A.,Carlson, N. M., and Smartt, H. B. 1989. Detection of Metal-Transfer Mode in GMAW, Recent Trends in Welding Science and Technology TWR'89, *Proceedings of the Second International Conference on Trends in Welding Research,* Gatlinburg, Tenn., pp.377-381.

6. Lesnewich, A. 1958. Control of melting rate and metal transfer in gas shielded metal arc welding, part II—control of metal transfer. *Welding Journal* 37(4):418-s to 425-s.

7. Johnson, J. A., et al. 1986. Automated welding process sensing and control. *Proceedings of the Second International Symposium on the Nondestructive Characterization of Materials,* New York: Plenum Publishing Corp., pp. 409-417.

8. Richardson, R. W., Gutow, D. A., Anderson, R. A., and Farson, D. A. 1984. Coaxial arc weld pool monitoring for process monitoring and control. *Welding Journal* 63(3):43-50.

9. Carlson, N. M., and Johnson, J. A. 1988. Ultrasonic sensing of weld pool penetration. *Welding Journal* 67(11):239-s to 246-s.

10. Lott, L. A. 1984. Ultrasonic detection of molten/solid interfaces of weld pools. *Materials Evaluation* 42, p. 337.

11. Hardt, D. E., and Katz, J. M. 1984. Ultrasonic measurement of weld penetration. *Welding Journal* 63(9):273-s to 281-s.

12. Stroud, R. R., and Fenn, R. 1985. The measurement and control of penetration during submerged arc welding. *Welding Journal* 64:18-22.

13. Deam, R. T. 1989. Weldpool frequency: a new way to define a weld procedure, Recent Trends in Welding Science and Technology TWR'89, *Proceedings of the Second International Conference on Trends in Welding Research,* Gatlinburg, Tenn., pp. 967-971.

14. Rohklin, S., Cho, K., and Gun, A. C. 1989. Closed-loop process control of weld penetration using real-time radiography. *Materials Evaluation* 47, pp. 363-369.

15. Smartt, H. B., Einerson, C. J., Watkins, A. D., and Morris, R. A. 1986. Gas metal arc process sensing and control. Advances in Welding Science and Technology TWR'86, *Proceedings of the First International Conference on Trends in Welding Research,* Gatlinburg, Tenn., pp. 461-465.

16. Doumanidis, C. C., and Hardt, D. E. 1988. A model for in-process control of thermal properties during welding. *Trans. ASME, J. Dynamic Systems, Measurements and Control.*

17. Kim, Y. S., and Eagar, T. W. 1989. Temperature distribution and energy balance in the electrode during GMAW. *Recent Trends in Welding Science and Technology TWR'89,* Proceedings of the Second International Conference on Trends in Welding Research, Gatlinburg, Tenn., pp. 13-18.

18. Johnson, J. A., Carlson, N. M., and Smartt, H. B. 1986. *Gas Metal Arc Defect Formation Mechanisms: Detection and Control,* EGG-SD-7405.

19. Johnson, J. A., et al. 1988. Ultrasonic and video computerized data acquisition for automated welding. *Proceedings of the 2nd International Conference on Computer Technology in Welding,* The Welding Institute, Cambridge, England, pp. 18-1 to 18-9.

20. Johnson, J. A., et al. 1987. A CAMAC based ultrasonic data acquisition workstation. *Materials Evaluation* 45, pp. 934-938.

21. Johnson, J. A., Carlson, N. M., Lott, L. A. 1987. Ultrasonic wave propagation in temperature gradients. *Journal of NDE* 6, No. 3, pp. 147-157.

22. Johnson, J. A., and Tow, D. M. 1986. Numerical calculations of ultrasonic field/crack interactions. *Review of Progress in Quantitative NDE,* 5A, D. O. Thompson and D. E. Chimenti, eds., New York: Plenum Publishing Corp., pp. 83-91.

23. Kurz, W., and Lux, B. 1969. *Berg-und Huttenmannische Monatshefte* 114, p. 123-130.

24. Johnson, J.A., Carlson, N.M. 1986. Weld energy reduction by using concurrent nondestructive evaluation. *NDT International* 19, pp.190-196.

25. Stroud, R. Seam tracking with ultrasound, preprint, private communication.

26. Johnson, J. A., and Carlson, N. M. 1988. Noncontact Ultrasonic Sensing of Weld Pools for Automated Welding. Third International Symposium on Nondestructive Characterization of Materials, Saarbruecken, FRG.

WRC Bulletin 332
April 1988

This Bulletin contains two reports that characterize the mechanical properties of two different structural shapes of constructional steels used in the pressure vessel industry.

(1) Characteristics of Heavyweight Wide-Flange Structural Shapes
By J. M. Barsom and B. G. Reisdorf

This report presents information concerning the chemical, microstructural and mechanical (including fracture toughness) properties for heavyweight wide-flange structural shapes of A36, A572 Grade 50 and A588 Grade A steels.

(2) Data Survey on Mechanical Property Characterization of A588 Steel Plates and Weldments
By A. W. Pense

This survey report summarizes, for the most part, unpublished data on the strength toughness and weldability of A588 Grade A and Grade B steels as influenced by heat treatment and processing.

Publication of this Bulletin was sponsored by the Subcommittee on Thermal and Mechanical Effects on Materials of the Pressure Vessel Research Committee of the Welding Research Council. The price of WRC Bulletin 332 is $20.00 per copy, plus $5.00 for postage and handling. Orders should be sent with payment to the Welding Research Council, Suite 1301, 345 E. 47th St., New York, NY 10017.